Electronic Supplementary Material (ESI) for Dalton Transactions.
This journal is © The Royal Society of Chemistry 2017

Supporting Information

A Luminescent Ratiometric pH Sensor Based on Nanoscale and Biocompatible Eu/Tb-Mixed MOF

Tifeng Xia, Fengliang Zhu, Ke Jiang, Yuanjing Cui*, Yu Yang and Guodong Qian*

State Key Laboratory of Silicon Materials, Cyrus Tang Center for Sensor Materials and Applications, School of Materials Science & Engineering, Zhejiang University, Hangzhou 310027, China

*Corresponding authors:

Yuanjing Cui: cuiyj@zju.edu.cn

Guodong Qian: gdqian@zju.edu.cn.

Table S1 The molar ratio of the starting Eu/Tb salt and that in mixed-lanthanide NMOF calculated by ICP analyses.

Sample	The molar ratio of the starting Eu/Tb salt	The Eu/Tb ratios calculated by ICP analysis
$Eu_{0.1}Tb_{0.9}$-NMOF	0.10:0.90	0.084:0.916
$Eu_{0.05}Tb_{0.95}$-NMOF	0.05:0.95	0.056:0.944
$Eu_{0.01}Tb_{0.99}$-NMOF	0.01:0.99	0.034:0.966
$Eu_{0.005}Tb_{0.995}$-NMOF	0.005:0.995	0.016:0.984

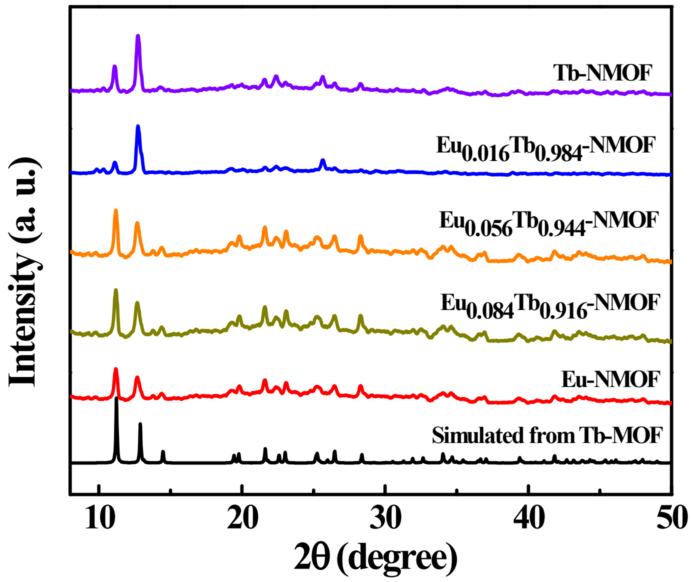

Fig. S1 PXRD patterns of **Eu-NMOF**, **Tb-NMOF**, **$Eu_{0.016}Tb_{0.984}$-NMOF**, **$Eu_{0.056}Tb_{0.944}$-NMOF**, and **$Eu_{0.084}Tb_{0.916}$-NMOF**.

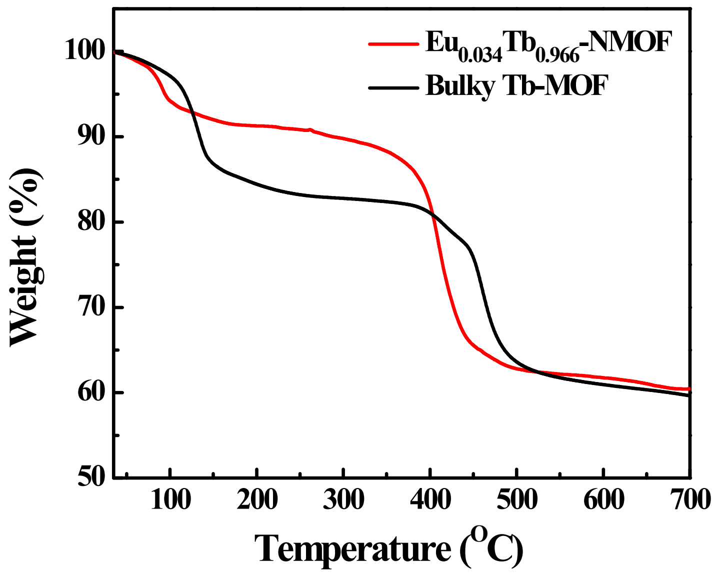

Fig. S2 The TGA curves of **$Eu_{0.034}Tb_{0.966}$-NMOF** and bulky Tb-MOF.

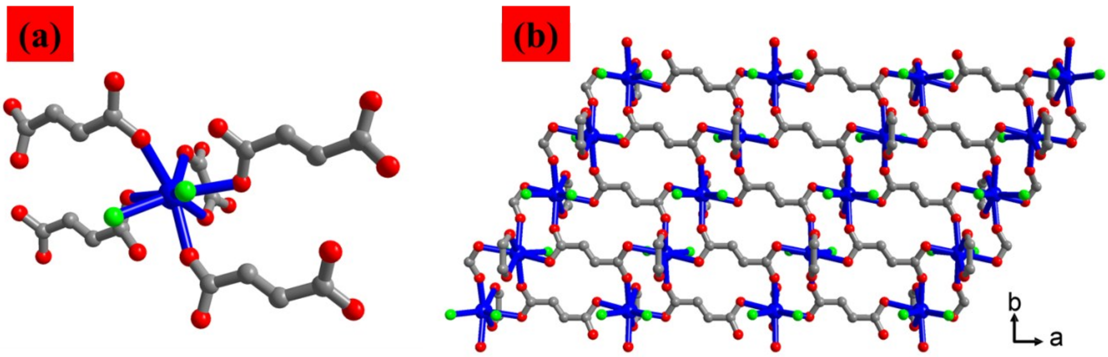

Fig. S3 The structure of $Ln_2(fum)_2(ox)(H_2O)_4$ (Ln = Eu, Tb): (a) local coordination environment of Ln ion and (b) two-dimensional Ln-fumarate layers viewed along the *c* axis. Color scheme: Ln, blue; C, gray; O of fumarate and oxalate, red; O of coordination water, green. H atoms are omitted for clarity.

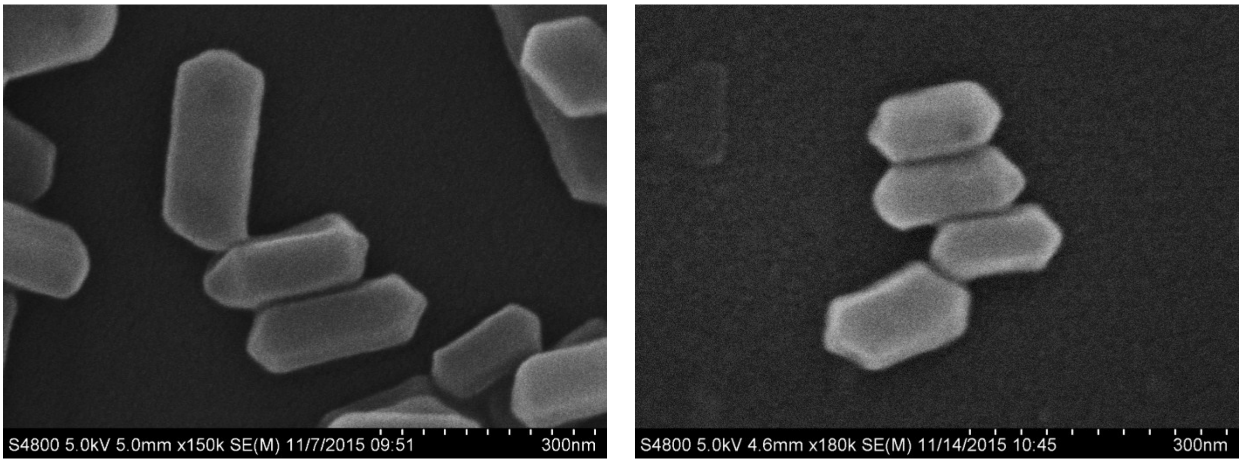

Fig. S4 SEM images of **$Eu_{0.034}Tb_{0.966}$-NMOF** morphologies synthesized with $W = 15$ (left) and $W = 10$ (right).

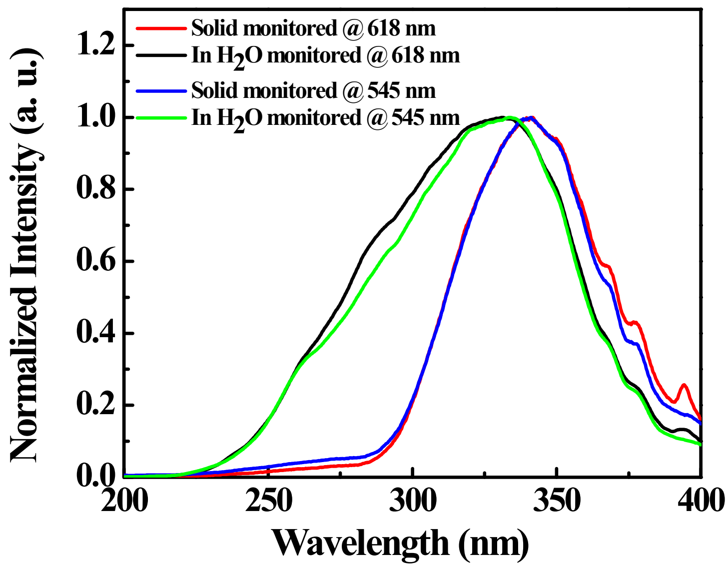

Fig. S5 Excitation spectra in the solid state monitored at 618 nm (red) and 545 nm (blue), and aqueous suspension monitored at 618 nm (black) and 545 nm (green) of **$Eu_{0.034}Tb_{0.966}$-NMOF**.

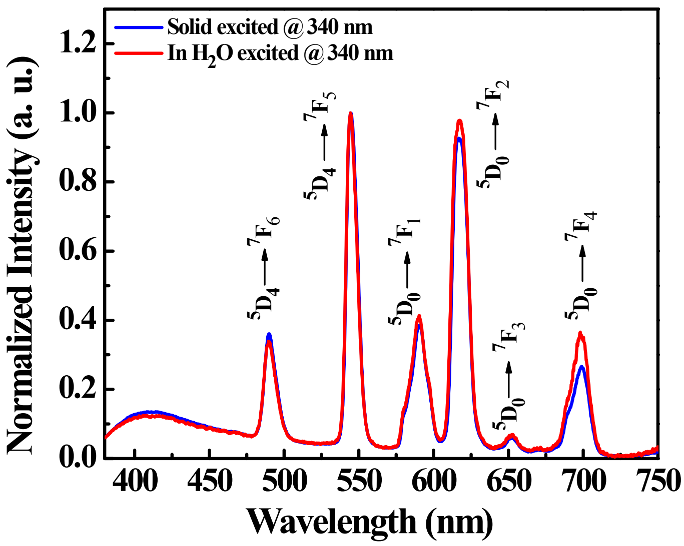

Fig. S6 Emission spectra excited at 340 nm of the solid state (blue) and aqueous suspension (red) of **$Eu_{0.034}Tb_{0.966}$-NMOF**.

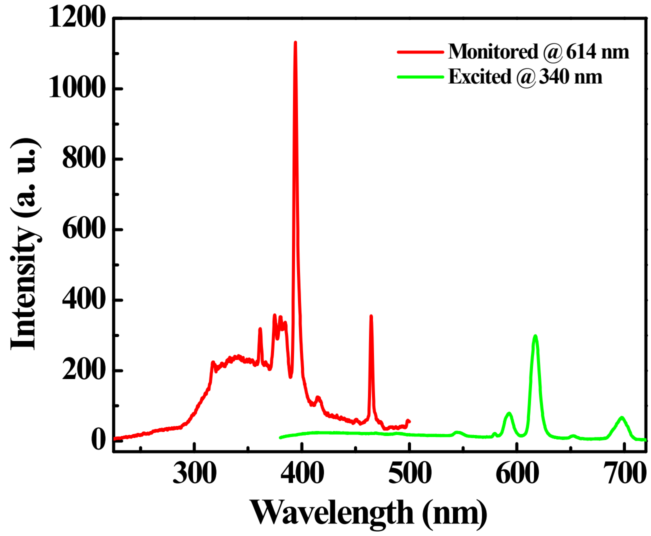

Fig. S7 Excitation and emission spectra of **Eu-NMOF** in the solid state.

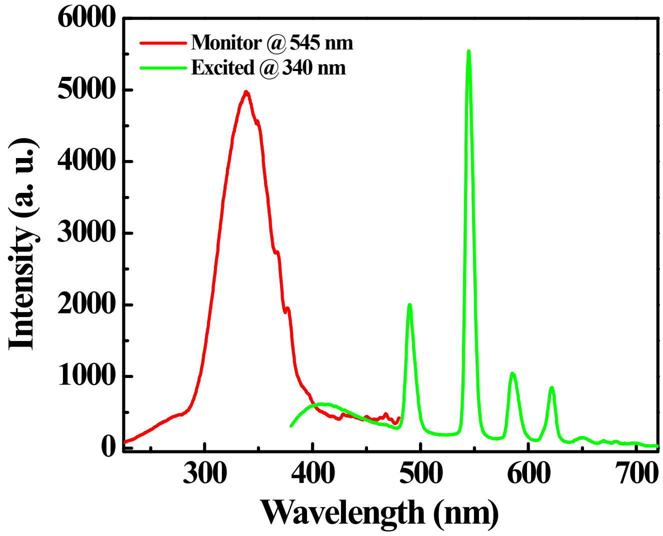

Fig. S8 Excitation and emission spectra of **Tb-NMOF** in the solid state.

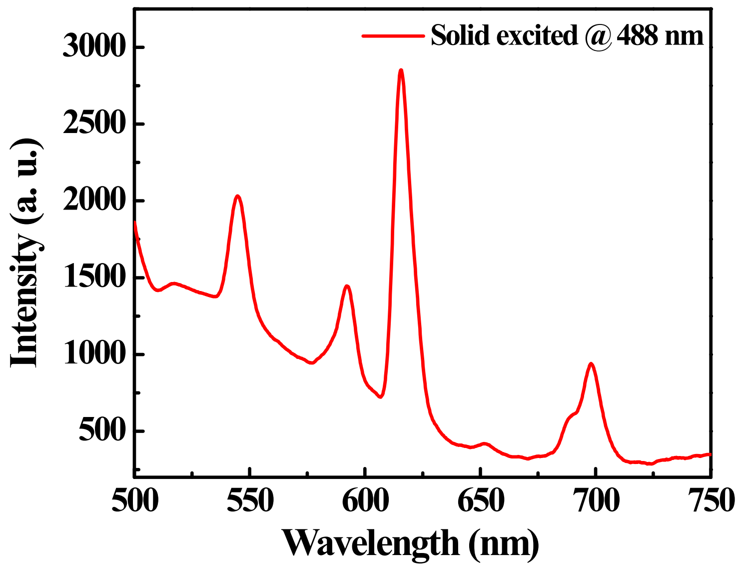

Fig. S9 Emission spectrum of **$Eu_{0.034}Tb_{0.966}$-NMOF** excited at 488 nm in solid state.

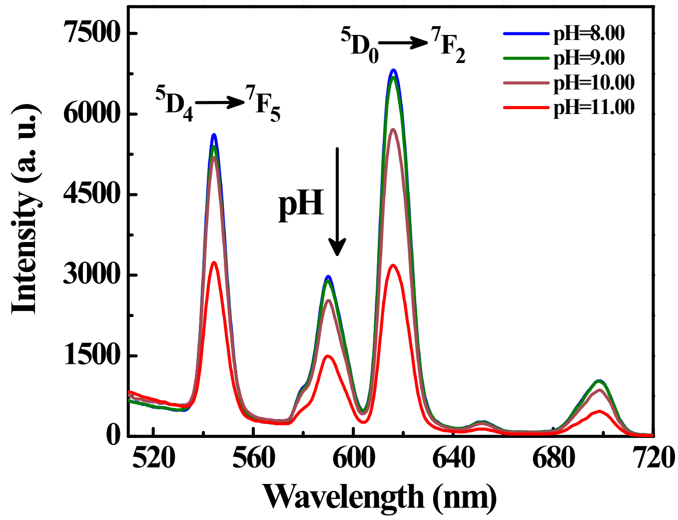

Fig. S10 pH-dependent emission spectra (λ_{ex} = 340 nm) of **$Eu_{0.034}Tb_{0.966}$-NMOF** in the pH ranging from 8.00 to 11.00.

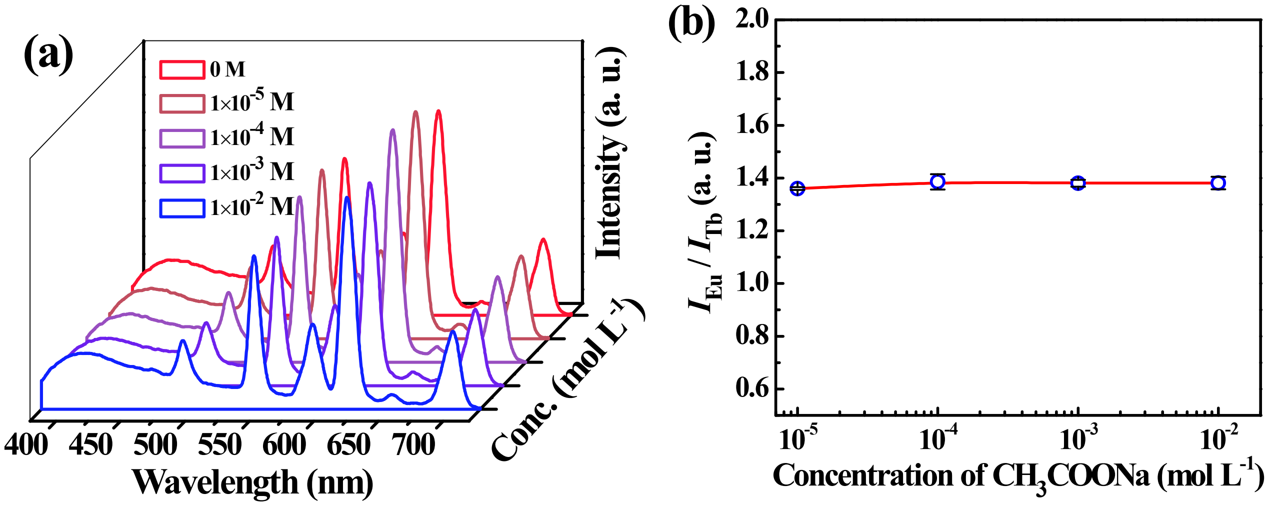

Fig. S11 Emission spectra (a) and intensity ratio (b) of **$Eu_{0.034}Tb_{0.966}$-NMOF** in aqueous solution with different concentration of CH_3COONa. The pH value of all solutions is 7.00.

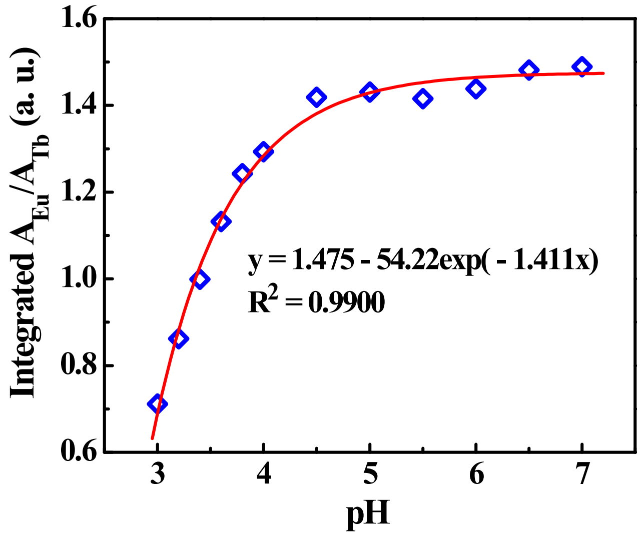

Fig. S12 pH-dependent integrated area ratio of $^5D_0 \rightarrow {}^7F_2$ (Eu^{3+}) to $^5D_4 \rightarrow {}^7F_5$ (Tb^{3+}) and the fitting curve for **$Eu_{0.034}Tb_{0.966}$-NMOF** in the pH ranging from 3.00 to 7.00.

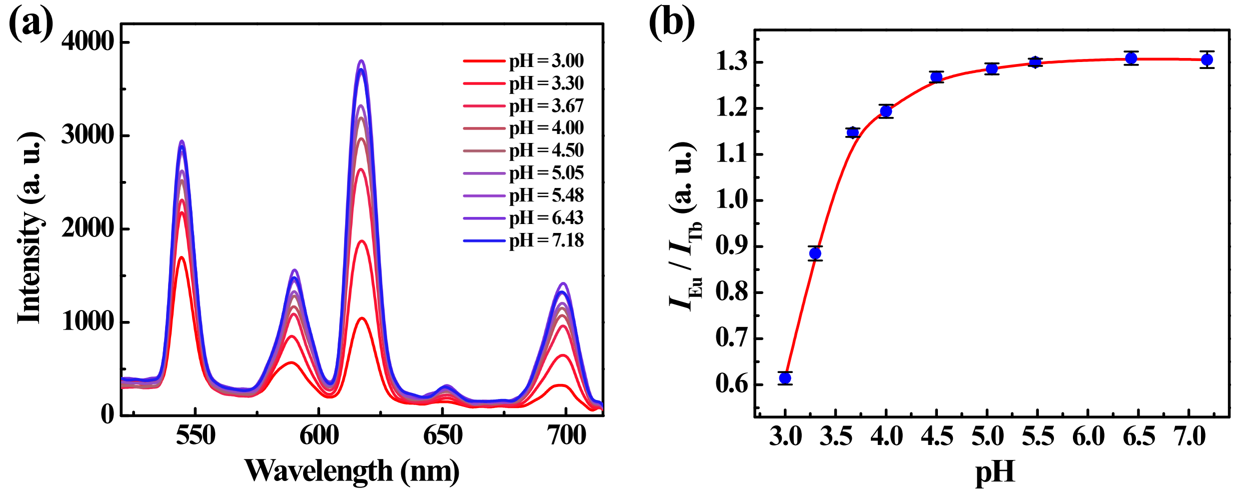

Fig. S13 pH-dependent emission spectra (a) and pH-dependent intensity ratio (b) of **$Eu_{0.034}Tb_{0.966}$-NMOF** with W = 10, which exhibits a negligible difference in property compared to the one with $W = 20$.

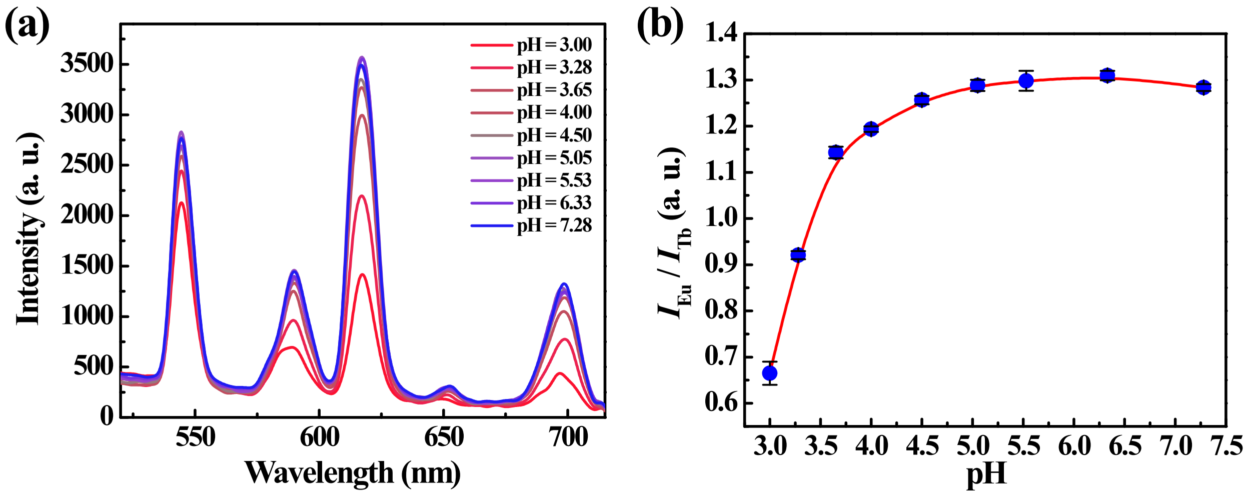

Fig. S14 pH-dependent emission spectra (a) and pH-dependent intensity ratio (b) of **$Eu_{0.034}Tb_{0.966}$-NMOF** in citric acid/NaOH system, which shows the universal applicability of this pH sensor in different buffer system with almost the same properties.

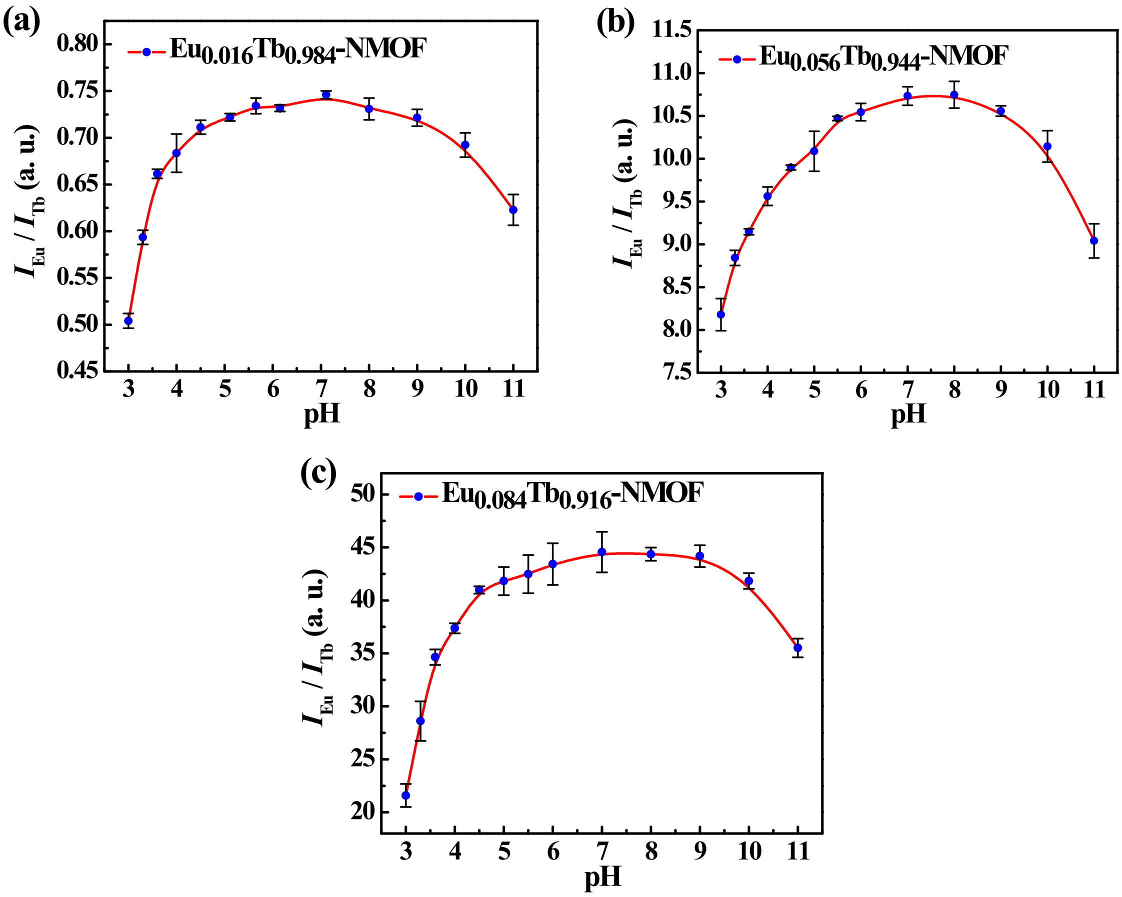

Fig. S15 pH-dependent intensity ratio of **$Eu_{0.016}Tb_{0.984}$-NMOF** (a), **$Eu_{0.056}Tb_{0.944}$-NMOF** (b) and **$Eu_{0.084}Tb_{0.916}$-NMOF** (c) in the pH ranging from 3.00 to 11.00.

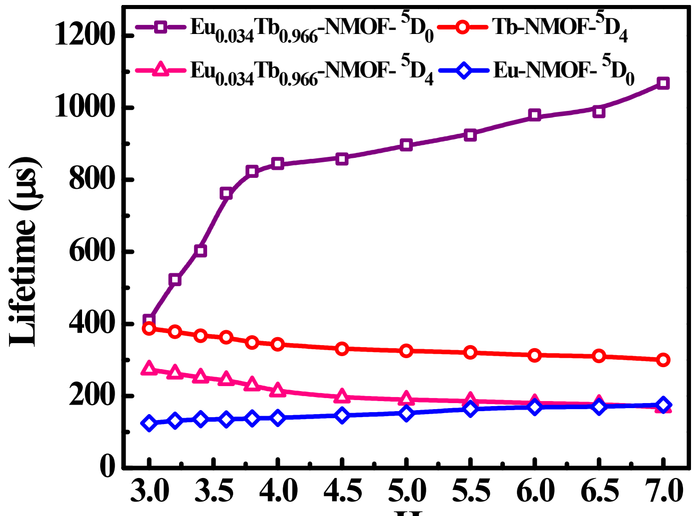

Fig. S16 pH-dependent lifetime of $^5D_4$ and $^5D_0$ in **Eu-NMOF**, **Tb-NMOF**, and **$Eu_{0.034}Tb_{0.966}$-NMOF**. The decay curves are monitored at 545 and 618 nm, respectively, and excited at 340 nm.

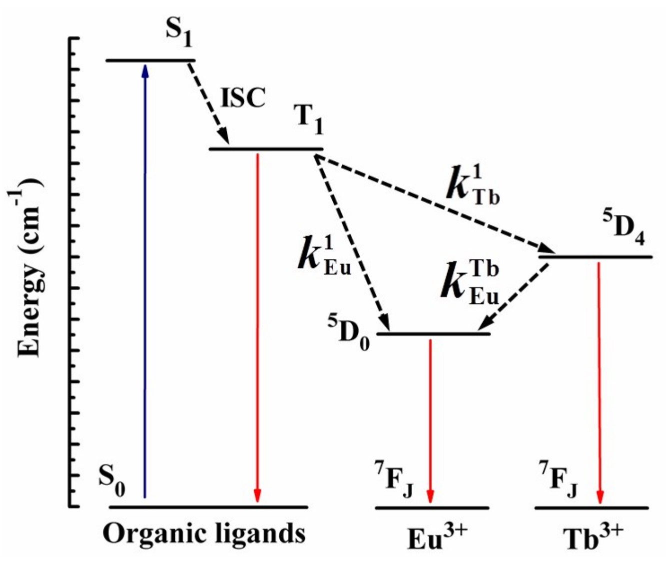

Fig. S17 The energy diagram and downconversion processes of Tb and Eu in mixed-lanthanide **Eu_xTb_{1-x}-NMOF**. Abbreviations: S = singlet; T = triplet; ISC = intersystem crossing; *k* = radiative or nonradiative transition probability. The solid arrows represent singlet−singlet absorption and radiative transitions; dotted arrows indicate nonradiative transitions.

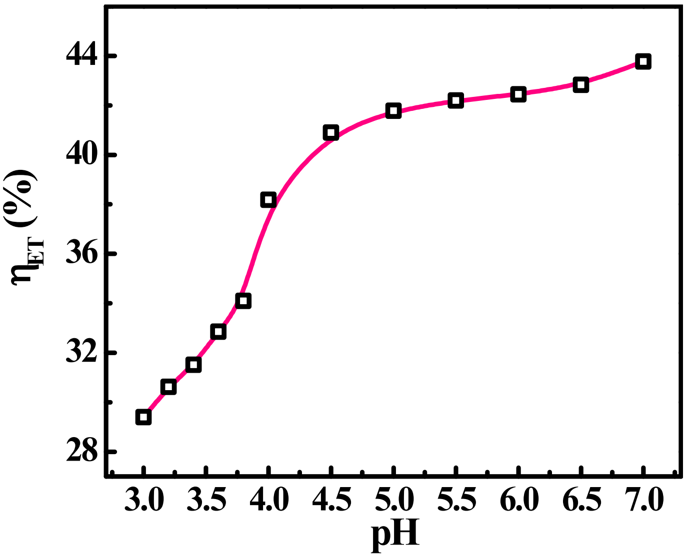

Fig. S18 pH-dependent Tb^{3+} to Eu^{3+} energy transfer efficiency (η_{ET}) in **$Eu_{0.034}Tb_{0.966}$-NMOF**. The pH range is varying from 3.00 to 7.00.

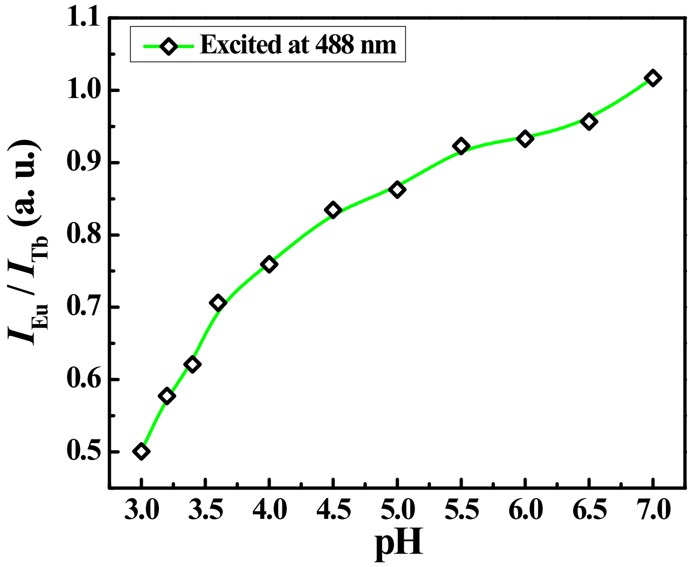

Fig. S19 Emission intensity ratio of Eu^{3+} (618 nm) to Tb^{3+} (545 nm) of **$Eu_{0.034}Tb_{0.966}$-NMOF** recorded within the pH ranging from 3.00 to 7.00, excited at 488 nm.

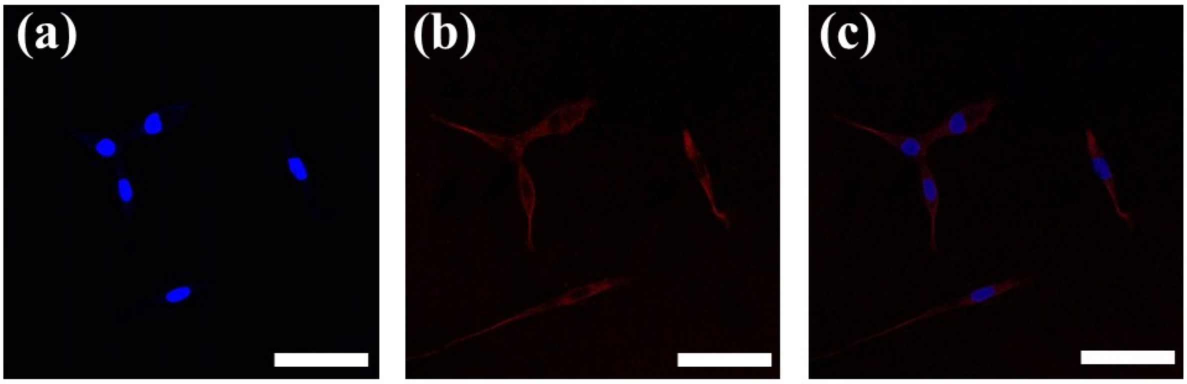

Fig. S20 (a, b) Fluorescence and (c) overlapped confocal microscopy images of fixed PC12 cells incubated with 50 µg mL^{-1} **$Eu_{0.034}Tb_{0.966}$-NMOF** for 6 hours. Microtubular cytoskeleton (tubulin, red) and nuclei (blue) were fluorescently stained. The scale bar is 50 µm.